ACS APPLIED MATERIALS & INTERFACES

Research Article

www.acsami.org

Self-Assembly Synthesis of N-Doped Carbon Aerogels for Supercapacitor and Electrocatalytic Oxygen Reduction

Junli Zhang,[†] Gaoli Chen,[†] Qian Zhang,[‡] Fei Kang,[†] and Bo You*[,†]

[†]Department of Chemistry, University of Science and Technology of China, Hefei, Anhui 230026, China

[‡]Department of Chemistry and Biochemistry, Utah State University, Logan, Utah 84322-0300, United States

Supporting Information

ABSTRACT: The rational design of high-performance and cheap nanomaterials for multiple sustainable energy storage applications is extremely urgent but remains challenging. Herein, a facile commercial melamine-sponge-directed multicomponent surface self-assembly strategy has been reported to synthesize N-doped carbon aerogels (NCAs) with low density (0.01 g cm^{-3}), large open pores, and high surface area (1626 m^2 g^{-1}). The commercial melamine sponge simultaneously serves as a green N source for N-doping and a 3D scaffold to buffer electrolytes for reducing ion transport resistance and minimizing ion diffusion distance. With their tailored architecture characteristics, the NCAs-based supercapacitor and oxygen reduction electrocatalyst show excellent performance.

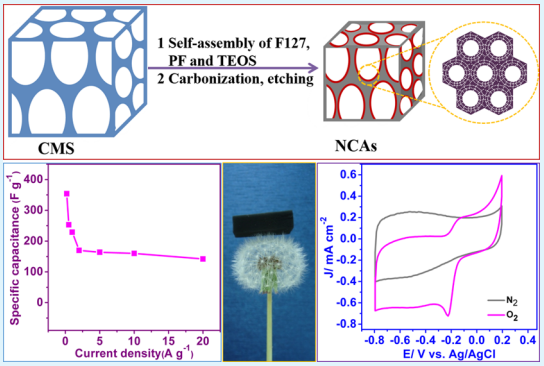

KEYWORDS: *nitrogen doping, carbon aerogels, supercapacitor, oxygen reduction, electrocatalysis*

INTRODUCTION

Since the first report of aerogels by Kistler in 1930s,[1] several light cellular materials such as oxide aerogels,[2] metal aerogels,[3] chalcogenide aerogels,[4] and carbon-based aerogels (CAs)[5−8] have been prepared to exploit their wide applications ranging from thermal insulators to heavy metals, oil absorption,[5,6] energy storage, and catalyst supports[7] due to their low density, large open pores, high inner surface area, and other excellent properties.[8] Specifically, CAs combining the high conductivity of nanocarbons with the aforementioned properties of aerogels have attracted intensive attention.[5−7,9] The true potential of CAs may be realized by introducing functional materials to achieve more advanced usability, such as oxygen reduction electrocatalysts and supercapacitors.[10,11]

In conjunction with the emergence of these new CAs, nitrogen (N) doping has been proven effective for improving the energy storage performance and electrocatalytic activities of nanocarbon materials.[14] In the N-doped electron-rich carbon nanostructures, carbon π electrons can be activated by conjugation with lone-pair electrons from N dopants, and the positively charged carbon atoms that are neighbor to N atoms can effectively reduce oxygen molecules.[15] Additionally, the N atoms, a pseudocapacitive component, concomitantly contribute to the improvement of the specific capacitance by coupling the pseudocapacitance to the electric double-layer capacitors of nanocarbons.[12−14] Up until now, the reported methods for N-doped nanocarbon mainly included chemical vapor deposition, arc discharge, thermal annealing with N precursors, and so on.[16] Rigorous conditions or special instruments are often required. Also, the toxic N-enriched small molecules, such as NH_3, aniline, pyridine, pyrrole, or melamine, have been used.[16] For example, our group recently reported a hydrothermal self-assembly strategy to fabricate 3D N-doped graphene−CNT networks (3D-NGCs) in the presence of pyrrole. The resulting 3D-NGCs-based supercapacitors show high specific capacitance, good rate capability, and excellent stability.[13] However, the toxicity of these N precursors limits the practical applications.[17] It is still of great urgency to develop relatively green and facile methods to synthesize novel N-doped nanocarbon materials with superior electrochemical performance.

In this work, we report a relatively green and facile self-assembly approach for the synthesis of N-doped carbon aerogels (NCAs), a multicomponent self-assembly on the surface of commercial melamine sponge (CMS). The key difference of this new approach is that we used CMS, a melamine polymer, as a green N precursor and a 3D substrate for the self-assembly. The CMS, discovered in the early 21st century, is an effective abrasive cleaner and has been used for over 20 years. For instance, Hou's group synthesized an elastic carbon foam by directly carbonizing commercial melamine foam, which functioned well as flexible electrode and organic adsorbent.[18] The CMS is inexpensive, easy to obtain, and nontoxic at room temperature.[18] Importantly, the 3D interconnected macrostructures can buffer electrolytes to reduce ion transport resistance and minimize ion diffusion

Received: February 22, 2015
Accepted: May 29, 2015
Published: May 29, 2015

DOI: 10.1021/acsami.5b01660
ACS Appl. Mater. Interfaces 2015, 7, 12760−12766

distance for enhanced applications. The large amounts of macropores and interconnected mesopores with high surface area promote ion transport and charge storage.[19,20] Benefiting from the synergistic effects, the resulting NCAs show excellent capacitance and advanced oxygen reduction properties.

EXPERIMENTAL SECTION

Materials. Tetraethyl orthosilicate (TEOS), phenol, formaldehyde solution (37%), NaOH, HCl, and ethanol were purchased from Sinopharm Chemical Reagent Co., Ltd. Pluronic F127 (MW = 12 600, PEO_{106}–PPO_{70}–PEO_{106}) was purchased from Sigma-Aldrich Corp. All chemicals were used as received without any further purification. Doubly distilled water was used in all experiments.

Synthesis of the N-Doped Carbon Aerogels. In a typical preparation, a 0.5 g block of the copolymer F127 was dissolved in a solution containing 2.0 g ethanol and 0.5 g HCl (0.2 M) and stirred for 1 h at 40 °C to afford a clear solution. Next, 1.04 g of TEOS and 1.25 g of 20 wt % phenol-formaldehyde resol (PF)−ethanol solution were added in sequence. After being stirred for 90 min, the commercial melamine sponges were added into the mixture, followed by the evaporation of ethanol for 8 h at room temperature. The hybrids were then subjected to thermopolymerization at 100 °C for 24 h. Finally, the as-made specimens were calcined in a tubular furnace at 850 °C for 2 h under Ar, followed by NaOH etching for the removal of silica; thus, the NCAs were obtained.

Synthesis of the Control Samples. The preparation of mesoporous carbon (MC) is similar to that of NCAs even without the addition of CMS; the carbonized melamine foam (MF) was prepared by the direct carbonization of the CMS at 850 °C for 2 h under Ar.

Characterization. Transmission electron microscopy (TEM) measurements were taken on a JEOL 2100F microscope (JEM, Japan) operated at 200 kV. Scanning electron microscopy (SEM) measurements were taken on a Sirion 200 microscope (FEI, USA) operated at 5 kV. Nitrogen sorption isotherms were measured at 77 K with a Micromertics ASAP 3020 analyzer (Micromertics, USA). Before measurements were taken, the samples were degassed in a vacuum at 300 °C for at least 5 h. The Brunauer−Emmett−Teller (BET) method was utilized to calculate the specific surface areas (S_{BET}) using adsorption data in a relative pressure range from 0.04 to 0.2. By using the Barrett−Joyner−Halenda (BJH) model, we derived the pore volumes and pore size distributions from the adsorption branches of isotherms, and the total pore volumes (V_t) were estimated from the adsorbed amount at a relative pressure (P/P_0) of 0.994. The X-ray photoelectron spectra (XPS) were recorded on an ESCALab MKII X-ray photoelectron spectrometer using a Mg Kα radiation exciting source.

Electrochemical Measurement. *Evaluation of the Supercapacitor Properties.* The electrochemical properties of the prepared samples were investigated with a CHI 660A electrochemical workstation (Chenhua, Shanghai) in 6 M KOH using cyclic voltammetry (CV) and galvanostatic charge−discharge methods in a conventional three-electrode cell between −1.0 and 0.0 V, respectively, at various scan rates and current densities. The resulting NCAs were directly used as working electrodes. The Ag/AgCl and Pt wire were used as the reference and counter electrode, respectively. Specific capacitances derived from galvanostatic charge−discharge tests can be calculated from the equation:

$$C = I\Delta t/m\Delta V$$

where C, I, Δt, m, and ΔV are the specific capacitance (F g^{-1}), the discharge current (A), the discharge time (s), the mass of the active materials (g), and the potential window, respectively.

Electrochemical impedance spectroscopy (EIS) testing was performed in the frequency range from 0.1 Hz to 100 kHz with a bias potential of 0 V versus Ag/AgCl.

Electrocatalytic Oxygen Reduction Testing. Inks of the resulting samples (NCAs, MC and MF) were prepared by ultrasonically mixing 4 mg catalyst powder with a mixture of 960 uL ethanol and 40 uL Nafion solution (5 v/v %, Sigma-Aldrich) for 20 min to form homogeneous catalysts ink. Next, 10 μL of catalysts ink was carefully dropped onto the polished glassy carbon rotating disk electrode (RDE), leading to the mass loading of approximately 0.2 mg cm^{-2}. For comparison, the commercial Pt/C catalysts (Vulcan, 20 wt %) with a loading of approximately 25 μg cm^{-2} were employed.

Electrochemical measurements of cyclic voltammetry on RDE were performed by a computer-controlled IM6ex electrochemical workstation (Zahner, Germany) with a three-electrode cell system. A glass carbon RDE (PINE, 5 mm diameter, 0.196 cm^2), after the electrocatalyst was loaded, was used as the working electrode, an Ag/AgCl electrode as the reference electrode, and a Pt wire as the counter electrode. The electrochemical experiments were conducted in O_2-saturated 0.1 M KOH electrolyte for the oxygen reduction reaction at room temperature. The potential range is cyclically scanned between +0.2 and −0.8 V versus Ag/AgCl at a scan rate of 10 mV s^{-1} and various rotating speeds from 600 to 2000 rpm. The sample was tested three times to avoid any incidental error.

The Koutecky−Levich plots were obtained by the linear fitting of the reciprocal rotating speed versus the reciprocal current density collected at different potentials from −0.4 to −0.8 V versus Ag/AgCl. The overall electron transfer numbers per oxygen molecule involved in a typical ORR process were calculated from the slopes of Koutecky−Levich plots using the following equation:

$$\frac{1}{J_d} = \frac{1}{J_k} + \frac{1}{B\omega^{1/2}}$$

where J_k is the kinetic current in amperes at a constant potential, ω is the electrode rotating speed in rpm, and B is the reciprocal of the slope, which was determined from the slope of Koutecky−Levich plots based on the Levich equation as follows:

$$B = 0.2n\cdot F\cdot \nu^{-1/6}\cdot C_{O_2}\cdot D_{O_2}{}^{2/3}$$

where n is the number of electrons transferred per O_2 molecule, F is the Faraday constant (96 485 C mol^{-1}), ν is the kinetic viscosity, and C_{O_2} is the concentration of O_2 (1.2×10^{-3} mol L^{-1}). D_{O_2} is the diffusion coefficient of O_2 in 0.1 M KOH (1.9×10^{-5} cm s^{-1}), and the constant 0.2 is adopted when the rotating speed is in rpm.

The accelerated stability tests were performed in O_2-saturated 0.1 M KOH at room temperature by potential cycling between +0.2 and −0.8 V versus Ag/AgCl at a sweep rate of 200 mV s^{-1} for 10 000 cycles. At the end of cycling, the resulting electrode was used for polarization testing.

DOI: 10.1021/acsami.5b01660
ACS Appl. Mater. Interfaces 2015, 7, 12760−12766

RESULTS AND DISCUSSION

The overall synthetic procedure for NCAs is illustrated in Scheme 1. The commercial melamine sponge (CMS) with 3D interconnected macroporous framework was used as the substrate for the surface self-assembly of the Pluronic F127 templates, PF solution, and TEOS precursors. After the carbonization and subsequent NaOH etching, the F127 surfactant were burned out, the CMS was transferred to a nitrogen source to account for the N doping into the amorphous carbon that derived from PF, the silicates were removed by NaOH, and, finally, the NCAs were successfully constructed. We speculate that the possible mechanism of nitrogen doping on carbon aerogels is as follows: (1) The triconstituent of Pluronic F127 surfactant, PF, and TEOS can attach to the surfaces of CMS through physical adsorption or $\pi-\pi$ interactions due to their conjugated structure. (2) During the high-temperature carbonization, the N source of CMS that attached with PF is more likely doped due to the defects and edges of porous carbon that derived from PF, or the CMS itself can form N-doped carbon, which is similar to that of N-doped graphene.[13]

Scheme 1. Fabrication of NCAs

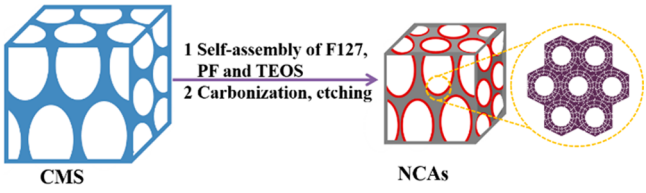

The as-prepared NCAs have an apparent density value of 0.01 g cm^{-3}, which is slightly lower than that of cellulose aerogel (0.14 g cm^{-3})[21] and of graphene aerogel (0.0109 g cm^{-3}).[22] The light weight allows an NCAs sample with a volume of approximately 3.9 cm^3 to stand stably on the top of a grass without deforming the grass at all (Figure 1a inset). The low density is directly ascribed to the rich, open, porous nanostructure, as shown in the SEM images (Figure 1a), which inherits the 3D interconnected macrostructures of CMS (Figure 1c) and MF (Figure 1d). The MC samples show a featureless morphology (Figure 1e), highlighting the important role of CMS. The thickness of the macropore wall for NCAs increases from approximately 5 to approximately 13 μm due to the coated mesoporous carbon derived from PF, an increase which is inverse to the decreased wall thickness of MF (from approximately 5 to approximately 3 μm) owing to shrinkage during the high-temperature carbonization of CMS (Figure 1d).

The high-resolution SEM (HR-SEM) of NCAs exhibits a clearly stripelike arrangement (Figure 1b) that is similar to that of MC samples (Figure 1f), implying an ordered nanostructure of NCAs and MC with 2D hexagonal pores (for more TEM images, see Figure S1 in the Supporting Information).[23] However, the MF only exhibits a smooth surface with no porosity (Figure 1d inset). The stripelike arrange is also observed from the TEM image (Figure 1g); the HR-TEM image (Figure 1g inset) shows that the pore size of these stripelike arranged pores is approximately 6 nm.[23] A comparison between the smooth surface of directly carbonized melamine foam (MF, Figure 1d) and the monolithic featureless morphology of mesoporous carbon (MC) without a 3D CMS substrate (Figure 1e) indicates that the hierarchical macro-mesoporous architecture of NCAs is ascribed to the synergistic effects between the CMS and the multicomponent self-assembly. The porosity of NCAs is further confirmed by N_2 sorption technology, as shown in Figure 1h. The NCAs exhibit a type IV isotherm with a sharp capillary condensation step in the relative pressure (P/P_0) ranging from 0.4 to 0.8 and an obvious H_2-type hysteresis loop corresponding to the narrow pore size distribution of large primary mesopores (approximately 6.0 nm) caused by the decomposition of F127 during carbonization.[24,25] The H_3-type hysteresis loop at P/P_0 between 0.8 and 1.0 is attributed to the macropores derived from CMS. Remarkably, a distinct sorption in the isotherm curves at P/P_0 in the range of 0.1−0.3 is observed, suggesting smaller pores with a wide distribution below 3.5 nm. The smaller pores interconnected with primary mesopores are attributed to the removal of silicas from TEOS.[26] Based on the standard BET method, the calculated specific surface area of

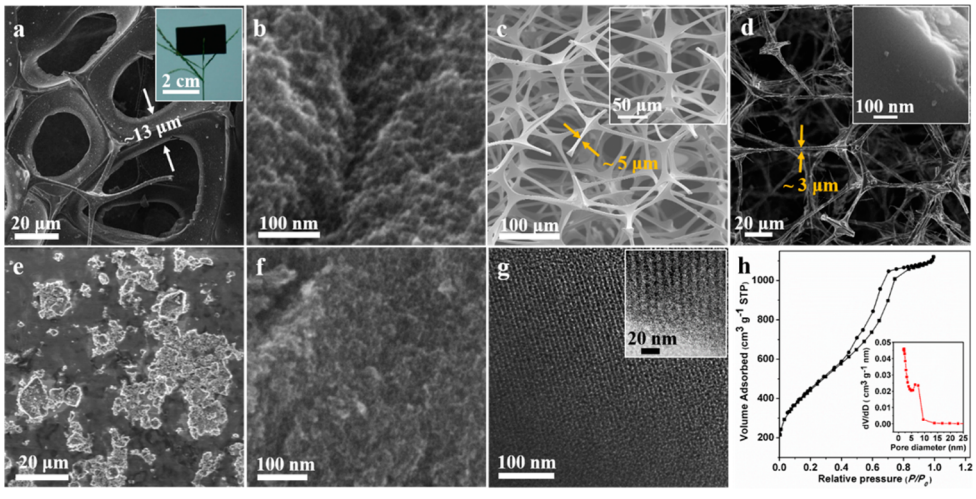

Figure 1. (a,c,e) SEM and (b,d,f) high-resolution SEM images of the (a,b) NCAs, (c) CMS, (d) MF, and (e,f) MC. (g) TEM images of NCAs. (h) N_2 sorption isotherms of NCAs. The insets of (a), (c), (d), (g), and (h) are the photographs of an as-prepared NCAs with a size of 2.7 cm × 1.6 cm × 0.9 cm standing on a grass, SEM images of CMS, the HR-SEM images of MF, HR-TEM images of NCAs, pore size distribution curves of NCAs, respectively.

DOI: 10.1021/acsami.5b01660
ACS Appl. Mater. Interfaces 2015, 7, 12760−12766

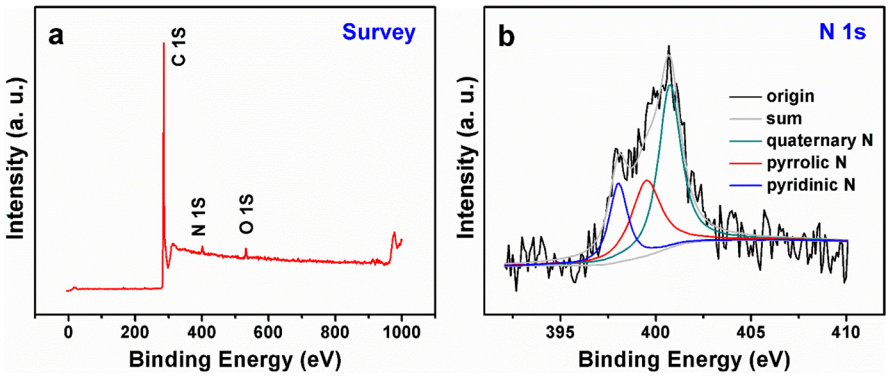

Figure 2. XPS spectra for the (a) survey scan and (b) N 1s region of the NCAs.

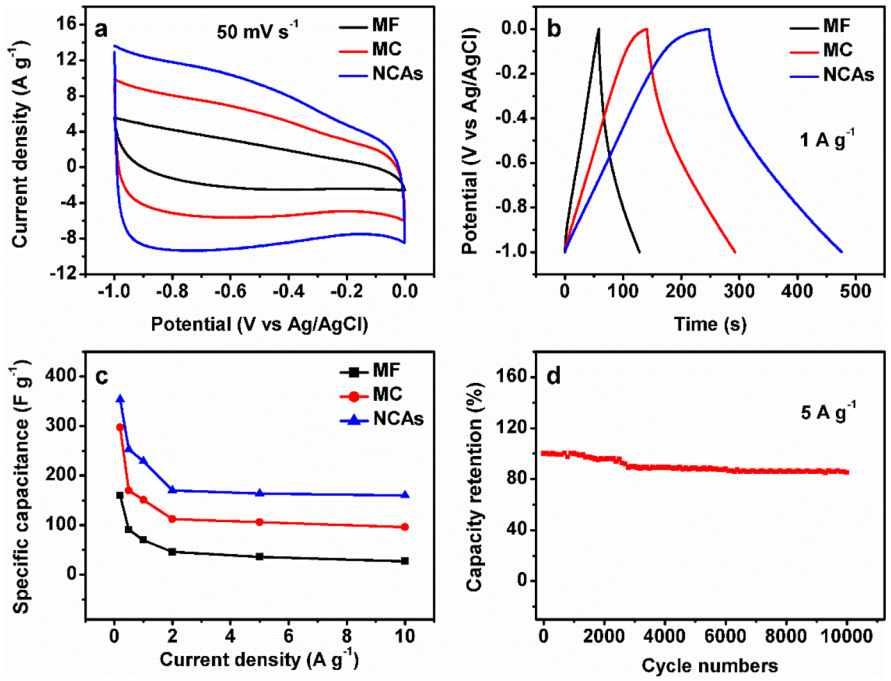

Figure 3. (a) Cyclic voltammetry and (b) Galvanostatic charge−discharge curves of MF, MC, and NCAs in 6 M KOH. (c) The variations of specific capacitances with current densities for MF, MC, and NCAs. (d) The cycling stability testing of NCAs in 6 M KOH at current density of 5 A g^{-1}.

NCAs is 1626 m^2 g^{-1} (which is higher than that of MF, MC, and other carbon-based aerogels, as shown in Figure S2 and Table S1 in the Supporting Information), and the total pore volume calculated based on the BJH model is 1.69 cm^3 g^{-1}. Primary pores with a diameter of 6.4 nm and complementary interconnected smaller pores (<3.5 nm) are also observed from the pore size distribution curve (Figure 1h inset), which is in good agreement with the TEM and N_2 sorption data.

The element chemical status of NCAs is investigated by X-ray photoelectron spectroscopy (XPS), as demonstrated in Figure 2. The survey spectrum of NCAs shows a primary graphitic C 1s peak at 285 eV and a pronounced N 1s peak at 402 eV (Figure 2a), along with an O 1s peak at 532 eV (Figure 2a), which verifies the doping of N atoms within CAs (2.0% N/C atomic ratio). The high-resolution N 1s spectrum (Figure 2b) of NCAs reveals the presence of pyridinic (398.2 eV), pyrrolic (399.5 eV), and quaternary (401.1 eV) nitrogen, all of which have been proven to be active in the oxygen reduction reaction (ORR) and supercapacitors.[27−31]

One of the most important applications of NCAs is as supercapacitor electrode materials for electrochemical energy storage. As shown in Figures 3a and S3 in the Supporting Information, the cyclic voltammetry (CV) curves of NCAs show a boxlike shape, evidently indicating the coexistence of an electric double-layer capacitance (EDLC) and pseudocapacitance due to redox reaction of pseudocapacitive N atoms.[11] In addition, the NCAs display higher current densities than MF and MC, representing higher capacitance.[11] These results clearly demonstrate the enhanced effect of N-doping and a 3D interconnected porous mesostructure. The 3D open interconnected porous frameworks increase the accessible surface area of the electrochemically active N atoms for charge transfer and reduce the ion diffusion length; the high surface area with macropores and large mesopores can also enhance the charge storage, rendering NCAs the highest capacitance. The galvanostatic discharge time for NCAs is significantly greater in comparison to that of the other two samples (Figures 3b and S4 in the Supporting Information). This data undoubtedly suggests that NCAs offer the largest charge capacity, which is consistent with the CV results (Figures 3a and S3 in the Supporting Information). Remarkably, the specific capacitance values versus the current densities as summarized in Figure 3c

DOI: 10.1021/acsami.5b01660
ACS Appl. Mater. Interfaces 2015, 7, 12760−12766

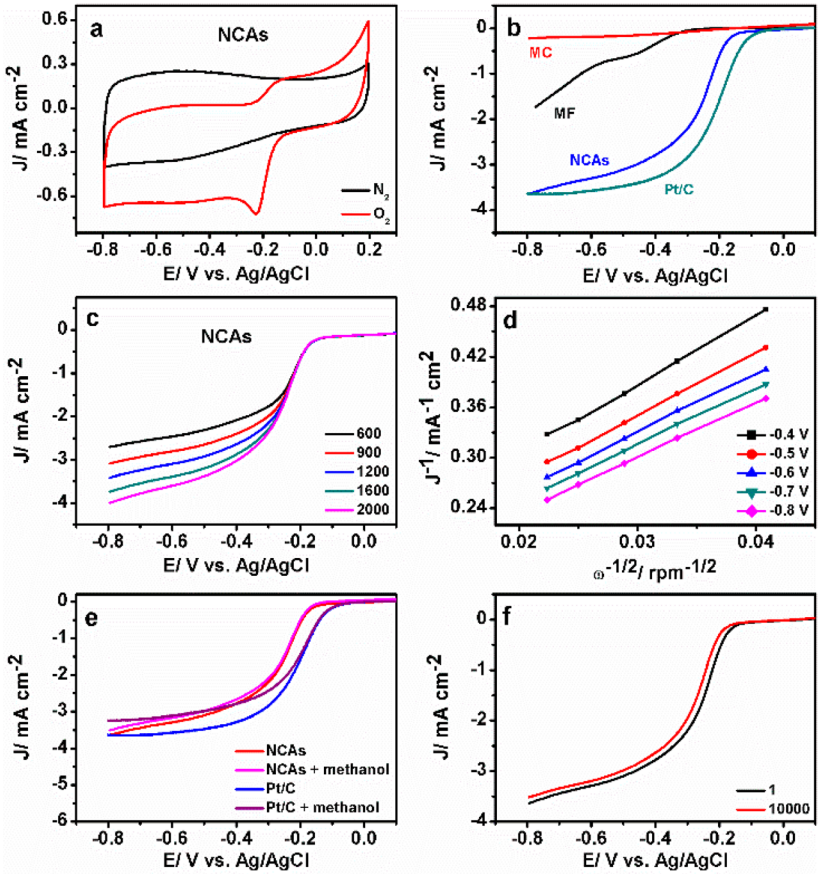

Figure 4. (a) Cyclic voltammetry curves of NCAs in O_2- or N_2-saturated electrolyte (0.1 M KOH) at scan rate of 10 mV s^{-1}. (b) Linear sweep voltammograms of different samples at 1600 rpm. (c) NCAs at a scan rate of 10 mV s^{-1} and different rotating speeds. (d) Koutecky–Levich plots of NCAs. (e) Linear sweep voltammograms of NCAs and Pt/C in O_2-saturated or 10 v/v % methanol 0.1 M KOH. (f) NCAs before and after 10 000 cycles at a scan rate of 200 mV s^{-1}.

indicate the improved capacitance and enhanced rate capability of NCAs compared to those of MC, MF, and other related materials (Table S2 in the Supporting Information). The highest specific capacitance for NCAs is 354 F g^{-1} at a current density of 0.2 A g^{-1}. Even when the current density increases to 10 A g^{-1}, the specific capacitance of 160 F g^{-1} still can be retained. We propose that the low Coulombic efficiency of NCAs at low current density is ascribed to the self-discharge phenomenon,[13] which is one of the drawbacks of supercapacitors and usually observed in the publications.[14] When the current density increases from 2 to 10 A g^{-1}, the specific capacitance of NCAs only drops approximately 5.8% (from 170 to 160 F g^{-1}), implying good conductivity and rate performance. Furthermore, the NCAs show excellent cycling stability, retaining approximately 85% of the initial specific capacitance even after 10 000 cycles at a current density of 5 A g^{-1}. The excellent capacitance properties are also confirmed by the electrochemical impedance spectroscopy (EIS) characterization (Figure S5 in the Supporting Information).

Furthermore, the NCAs can also be used as metal-free electrocatalysts for the oxygen reduction reaction, a critical but sluggish reaction happening on the cathode to derive fuel cells and metal–air batteries' work.[28−31] Different from the conventional 2D catalyst, NCAs provide unique 3D hierarchically porous frameworks with maximum access to the electrochemically active sites and multidimensional electron transport pathways. As shown in Figure 4a, a well-defined ORR peak at −0.23 V versus Ag/AgCl is observed within the O_2-saturated but not the N_2-saturated 0.1 M KOH solution for NCAs, in spite of the relatively high capacitive background of porous carbon.[28−31] The peak potential for NCAs is also comparable to that of other recently reported metal-free ORR catalysts that were tested under similar conditions, such as N-doped mesoporous graphene,[32] S-doped graphene,[33] and S- and N-codoped mesoporous graphene (−0.24 V versus Ag/AgCl),[30] indicating a similar ORR process. Different from the results for the MC and MF, the linear-sweep voltammograms (LSV) on a rotating disk electrode (RDE) for NCAs show a one-step process, suggesting a four-electron pathway for ORR as the case for the Pt/C catalyst (Figure 4b). Similar to that of other N-containing carbon catalysts,[28−33] the onset potential of NCAs is slightly lower than that of commercially available Pt–C. However, their diffusion current density is notably comparable to that of the Pt/C electrode at −0.8 V. LSV curves at various rotation speeds and Koutecky–Levich (K–L) plots with a good linear relationship for the NCAs are shown in Figure 4 (c) and (d), respectively. The electron-transferred number (n) per O_2 molecule determined from the K–L equation is 3.47, 3.49, 3.51, 3.51, and 3.52 at potentials of −0.4, −0.5, −0.6, −0.7, and −0.8 V versus Ag/AgCl, respectively, indicating that the ORR proceeds via a nearly four-electron pathway. The tolerance of NCAs to methanol crossover is assessed with LSV in comparison to that of the commercial Pt/C catalyst (Figure 4e). When 10 v/v % methanol is added into the testing cell, no obvious change of the ORR current for NCAs indicates a good tolerance to methanol, which is

DOI: 10.1021/acsami.5b01660
ACS Appl. Mater. Interfaces 2015, 7, 12760−12766

consistent with the chronoamperometric test (Figure S6 in the Supporting Information). While on Pt/C, the electro-oxidation of methanol retards the ORR process, as indicated by the large difference of the ORR current after adding the methanol. This fact indicates that the as-prepared NCAs are a nice alternative to a Pt/C cathode. Also, the accelerated durability tests were employed to evaluate the electrochemical stability of NCAs. After 10 000 continuous potential cycles, we noted a negative shift of only 24 mV about the half-wave potential ($E_{1/2}$) of NCAs (Figure 4f), which suggests the excellent durability and is lower than that of the reported metal−N-C electrocatalysts (32 mV) under similar testing conditions.[34]

CONCLUSIONS

In summary, we have demonstrated a relatively green and facile approach for the synthesis of N-doped carbon aerogels (NCAs) through the multicomponent self-assembly of F127, phenol-formaldehyde (PF) resol, and tetraethyl orthosilicate (TEOS) on the surface of commercial melamine sponge (CMS), wherein the CMS is used as a green N precursor and 3D substrate for self-assembly. The resulting N-doped carbon aerogels (NCAs) show low density (0.01 g cm^{-3}), large open pores, and high surface area (1626 m^2 g^{-1}). On the basis of the synergetic function of the 3D hierarchically porous frameworks and N doping, the NCAs supercapacitor shows a high specific capacitance of 354 F g^{-1} at a current density of 0.2 A g^{-1}, which is superior to that of the typical nanocarbon-based electrodes. Besides this, the NCAs exhibit excellent catalytic activity for the oxygen reduction reaction and superior methanol tolerance as well as robust durability. We believe that the NCAs also provide an important platform for other multiple applications, such as sensors and batteries.

ASSOCIATED CONTENT

Supporting Information

TEM images of the control samples, N_2 sorption isotherms and pore size distribution curves, cyclic voltammetry curves, galvanostatic charge/discharge curves, electrochemical impedance spectroscopy, comparison of the textural characteristics and specific capacitance of materials as well as chronoamperometric response. The Supporting Information is available free of charge on the ACS Publications website at DOI: 10.1021/acsami.5b01660.

AUTHOR INFORMATION

Corresponding Author

*E-mail: youbo@mail.ustc.edu.cn.

Author Contributions

J.Z. and G.C. contributed equally.

Notes

The authors declare no competing financial interest.

ACKNOWLEDGMENTS

We acknowledge the prof. Z. X. Deng and J. Yang for experimental support.

REFERENCES

(1) Kistler, S. S. Coherent Expanded Aerogels and Jellies. *Nature* **1931**, *127*, 741−741.

(2) Baena, J. P. C.; Agrios, A. G. Transparent Conducting Aerogels of Antimony-Doped Tin Oxide. *ACS Appl. Mater. Interfaces* **2014**, *6*, 19127−19134.

(3) Liu, W.; Herrmann, A. K.; Geiger, D.; Borchardt, L.; Simon, F.; Kaskel, S.; Gaponik, N.; Eychmüller, A. High-Performance Electrocatalysis on Palladium Aerogels. *Angew. Chem., Int. Ed.* **2012**, *51*, 5743−5747.

(4) Arachchige, I. U.; Brock, S. L. Sol-Gel Assembly of CdSe Nanoparticles to Form Porous Aerogel Networks. *J. Am. Chem. Soc.* **2006**, *128*, 7964−7971.

(5) Worsley, M. A.; Pauzauskie, P. J.; Olson, T. Y.; Biener, J.; Satcher, J. H.; Baumann, T. F. Synthesis of Graphene Aerogel with High Electrical Conductivity. *J. Am. Chem. Soc.* **2010**, *132*, 14067−14069.

(6) Sun, H. Y.; Xu, Z.; Gao, C. Multifunctional, Ultra-Flyweight, Synergistically Assembled Carbon Aerogels. *Adv. Mater.* **2013**, *25*, 2554−2560.

(7) Worsley, M. A.; Kucheyev, S. O.; Mason, H. E.; Merrill, M. D.; Mayer, B. P.; Lewicki, J.; Valdez, C. A.; Suss, M. E.; Stadermann, M.; Pauzauskie, P. J.; Satcher, J. H., Jr.; Biener, J.; Baumann, T. F. Mechanically Robust 3D Graphene Macroassembly with High Surface Area. *Chem. Commun.* **2012**, *48*, 8428−8430.

(8) Baumann, T. F.; Worsley, M. A.; Han, Y. J.; Satcher, J. H., Jr. High Surface Area Carbon Aerogel Monoliths with Hierarchical Porosity. *J. Non-Cryst. Solids* **2008**, *354*, 3513−3515.

(9) Wu, Z. Y.; Li, C.; Liang, H. W.; Chen, J. F.; Yu, S. H. Ultralight, Flexible, and Fire-Resistant Carbon Nanofiber Aerogels from Bacterial Cellulose. *Angew. Chem., Int. Ed.* **2013**, *52*, 2925−2929.

(10) Hamedi, M.; Karabulut, E.; Marais, A.; Herland, A.; Nysrom, G.; Wagberg, L. Nanocellulose Aerogels Functionalized by Rapid Layer-by-Layer Assembly for High Charge Storage and Beyond. *Angew. Chem., Int. Ed.* **2013**, *52*, 12038−12042.

(11) You, B.; Yin, P. Q.; An, L. N. Multifunctional Electroactive Heteroatom-Doped Carbon Aerogels. *Small* **2014**, *10*, 4352−4361.

(12) Wohlgemuth, S. A.; Vilela, F.; Titirici, M. M.; Antonietti, M. A One-Pot Hydrothermal Synthesis of Tunable Dual Heteroatom-Doped Carbon Microspheres. *Green Chem.* **2012**, *14*, 741−749.

(13) You, B.; Wang, L. L.; Yao, L.; Yang, J. Three Dimensional N-Doped Graphene−CNT Networks for Supercapacitor. *Chem. Commun.* **2013**, *49*, 5016−5018.

(14) Chen, L. B.; Bai, H.; Huang, Z. F.; Li, L. Mechanism Investigation and Suppression of Self-Discharge in Active Electrolyte Enhanced Supercapacitors. *Energy Environ. Sci.* **2014**, *7*, 1750−1759.

(15) Gong, K. P.; Du, F.; Xia, Z. H.; Durstock, M.; Dai, L. M. Nitrogen-Doped Carbon Nanotube Arrays with High Electrocatalytic Activity for Oxygen Reduction. *Science* **2009**, *323*, 760−764.

(16) Sheng, Z. H.; Shao, L.; Chen, J. J.; Bao, W. J.; Wang, F. B.; Xia, X. H. Catalyst-Free Synthesis of Nitrogen-Doped Graphene via Thermal Annealing Graphite Oxide with Melamine and Its Excellent Electrocatalysis. *ACS Nano* **2011**, *5*, 4350−4358.

(17) Wang, H. B.; Maiyalagan, T.; Wang, X. Review on Recent Progress in Nitrogen-Doped Graphene: Synthesis, Characterization, and Its Potential Applications. *ACS Catal.* **2012**, *2*, 781−794.

(18) Chen, S. L.; He, G. H.; Hu, H.; Jin, S. Q.; Zhou, Y.; He, Y. Y.; He, S. J.; Zhao, F.; Hou, H. Q. Elastic Carbon Foam via Direct Carbonization of Polymer Foam for Flexible Electrode and Organic Chemical Adsorption. *Energy Environ. Sci.* **2013**, *6*, 2435−2439.

(19) Lee, J. S.; Park, G. S.; Kim, S. T.; Liu, M. L.; Cho, J. A Highly Efficient Electrocatalyst for the Oxygen Reduction Reaction: N-Doped Ketjenblack Incorporated into Fe/Fe_3 C-Functionalized Melamine Foam. *Angew. Chem., Int. Ed.* **2013**, *52*, 1026−1030.

(20) Li, W.; Wu, Z. X.; Wang, J. X.; Elzatahry, A. A.; Zhao, D. Y. Tricomponent Coassembly Approach To Synthesize Ordered Mesoporous Carbon/Silica Nanocomposites and Their Derivative Mesoporous Silicas with Dual Porosities. *Chem. Mater.* **2014**, *26*, 2438−2444.

(21) Cai, J.; Liu, S. L.; Feng, J.; Kimura, S.; Wada, M.; Kuga, S.; Zhang, L. N. Cellulose−Silica Nanocomposite Aerogels by in Situ Formation of Silica in Cellulose Gel. *Angew. Chem., Int. Ed.* **2012**, *51*, 2076−2079.

(22) Hu, H.; Zhao, Z. B.; Wan, W. B.; Gogotsi, Y.; Qiu, J. S. Ultralight and Highly Compressible Graphene Aerogels. *Adv. Mater.* **2013**, *25*, 2219−2223.

DOI: 10.1021/acsami.5b01660
ACS Appl. Mater. Interfaces 2015, 7, 12760−12766

(23) Li, W.; Yue, Q.; Deng, Y. H.; Zhao, D. Y. Ordered Mesoporous Materials Based on Interfacial Assembly and Engineering. *Adv. Mater.* **2013**, *25*, 5129−5152.
(24) Li, W.; Zhao, D. Y. An Overview of the Synthesis of Ordered Mesoporous Materials. *Chem. Commun.* **2013**, *49*, 943−946.
(25) Li, W.; Zhang, F.; Dou, Y. Q.; Wu, Z. X.; Liu, H. J.; Qian, X. F.; Gu, D.; Xia, Y. Y.; Tu, B.; Zhao, D. Y. A Self-Template Strategy for the Synthesis of Mesoporous Carbon Nanofibers as Advanced Supercapacitor Electrodes. *Adv. Energy Mater.* **2011**, *1*, 382−386.
(26) You, B.; Yang, J.; Sun, Y. Q.; Su, Q. D. Easy Synthesis of Hollow Core, Bimodal Mesoporous Shell Carbon Nanospheres and Their Application in Supercapacitor. *Chem. Commun.* **2011**, *47*, 12364−12366.
(27) Wang, S.; Zhang, L.; Xia, Z.; Roy, A.; Chang, D. W.; Baek, J. B.; Dai, L. M. BCN Graphene as Efficient Metal-Free Electrocatalyst for the Oxygen Reduction Reaction. *Angew. Chem., Int. Ed.* **2012**, *51*, 4209−4212.
(28) Zheng, Y.; Jiao, Y.; Ge, L.; Jaroniec, M.; Qiao, S. Z. Two-Step Boron and Nitrogen Doping in Graphene for Enhanced Synergistic Catalysis. *Angew. Chem., Int. Ed.* **2013**, *52*, 3110−3116.
(29) Duan, J. J.; Zheng, Y.; Chen, S.; Tang, Y. H.; Jaroniec, M.; Qiao, S. Z. Mesopoeous Hybrid Materials of Mn_3O_4 Nanoparticles on Nitrogen-doped Graphene for Highly Efficient Oxygen Reduction Reaction. *Chem. Commun.* **2013**, *49*, 7705−7707.
(30) Liang, J.; Jiao, Y.; Jaroniec, M.; Qiao, S. Z. Sulfur and Nitrogen Dual-Doped Mesoporous Graphene Electrocatalyst for Oxygen Reduction with Synergistically Enhanced Performance. *Angew. Chem., Int. Ed.* **2012**, *51*, 11496−11500.
(31) Sun, Y. Q.; Li, C.; Shi, G. Q. Nanoporous Nitrogen Doped Carbon Modified Graphene as Electrocatalyst for Oxygen Reduction Reaction. *J. Mater. Chem.* **2012**, *22*, 12810−12816.
(32) Yuan, C. Z.; Wu, H. B.; Xie, Y.; Lou, X. W. Mixed Transition-Metal Oxides: Design, Synthesis, and Energy-Related Applications. *Angew. Chem., Int. Ed.* **2014**, *53*, 1488−1504.
(33) Yang, Z.; Yao, Z.; Li, G. F.; Fang, G. Y.; Nie, H. G.; Liu, Z.; Zhou, X. M.; Chen, X. A.; Huang, S. M. Sulfur-Doped Graphene as an Efficient Metal-Free Cathode Catalyst for Oxygen Reduction. *ACS Nano* **2012**, *6*, 205−211.
(34) Liu, J.; Sun, X. J.; Song, P.; Zhang, Y. W.; Xing, W.; Xu, W. L. High-Performance Oxygen Reduction Electrocatalysts Based on Cheap Carbon Black, Nitrogen, and Trace Iron. *Adv. Mater.* **2013**, *25*, 6879−6883.

DOI: 10.1021/acsami.5b01660
ACS Appl. Mater. Interfaces 2015, 7, 12760−12766